Hybrid porous Helmholtz resonator for low-frequency broadband absorption

Zihao Su,[1] Qing Wang,[2] Ze-Guo Chen,[1,3,*] and Ming-Hui Lu[1,3,4]

[1] *School of Materials Science and Intelligent Engineering, Nanjing University, Suzhou 215163, China*
[2] *School of Physical Science and Technology, ShanghaiTech University, Shanghai 201210, China*
[3] *National Laboratory of Solid State Microstructures, Nanjing University, Nanjing 210093, China*
[4] *College of Engineering and Applied Sciences, Nanjing University, Nanjing 210093, China*

(Received 4 June 2024; revised 27 August 2024; accepted 19 September 2024; published 11 October 2024)

The effective control of low-frequency noise remains a formidable challenge due to the inherently long wavelengths involved, which typically require large-scale physical barriers to achieve meaningful attenuation. Against this backdrop, metamaterials present a viable alternative, exploiting deep subwavelength structures that capitalize on thermal losses associated with local resonances to dampen sound. Here, we introduce a hybrid porous Helmholtz resonator (HPHR) that markedly improves acoustic absorption by amalgamating the Helmholtz resonator with specially designed porous necks to optimize acoustic impedance matching. It is promising as the basic unit of the metamaterial for low-frequency broadband acoustic absorption. Based on parallel HPHRs, we expand the effective absorption (>0.8) bandwidth using a one-dimensional convolutional neural network to engineer composite structures. The thickness of the sample is approximately 1/13th of the wavelength at the lowest target frequency. Our designs integrate resonant structures and porous materials, providing promising potential for creating broadband acoustic absorption systems and low-frequency noise control.

DOI: 10.1103/PhysRevApplied.22.044032

I. INTRODUCTION

The pervasive issue of low-frequency noise pollution significantly impacts urban and industrial environments, affecting human health and productivity. Traditional noise-mitigation strategies, such as large-scale barriers or porous materials [1–4], are often impractical due to their size, cost, and limited effectiveness at low frequencies under the constraints of the mass density law [5,6]. Metamaterials have offered unparalleled opportunities for sound manipulation at dimensions significantly smaller than the wavelength of the sound [7–10]. For instance, effective acoustic absorption using decorated membranes [11–13], Helmholtz resonator (HR) [14–18], and Fabry-Perot resonator [19–21] have been proposed. The HR stands out among various units due to its ample tunable parameters and degrees of freedom. To enhance the acoustic absorption of the HR, sophisticated designs are applied to the neck of the HR, e.g., the roughness will hinder the flow of the fluid in the neck, resulting in energy damping and dissipation [22–24]. Meanwhile, porous materials, inherently characterized by their roughness and viscosity, have also garnered renewed attention for their ability to dampen sound. It is an ideal candidate for improving metamaterial performance without altering the geometric parameters [25–28]. Recently, applying porous linings within the HR cavity has shown significant absorption properties [29–32]. Given that the neck is a primary site for energy dissipation, incorporating porous materials directly into the neck is a promising and more cost-effective approach. To date, this method's feasibility has not been experimentally verified. This study introduces a hybrid porous Helmholtz resonator (HPHR), which enhances traditional HR designs by incorporating a porous rectangular embedded neck. A refined theoretical model and complex frequency-plane analysis [33] elucidate the absorption improvements from impedance matching provided by the porous neck. Finite-element simulations support this finding.

Considering the nonlocal effects [34–36] that couple the adjacent units will bring another perspective to achieve broadband acoustic absorption, in which the design of each unit is neighbor dependent. Thus, utilizing nonlocal effects requires complex parameter sets. In this study, we developed a broadband acoustic metamaterial absorber utilizing parallel HPHRs that was optimized by deep learning. Kaleidoscopic structural designs in metamaterials allow for precise acoustic property control, offering alternative solutions for noise pollution across various settings. The deep-learning (DL) method is a powerful computational tool for efficiently addressing a wide range of scientific challenges, including in metamaterials [37–41]. By utilizing trained deep-learning models, it is possible to uncover

*Contact author: zeguoc@nju.edu.cn

the underlying relationships between the structural parameters and performance, enabling the inverse design of broadband acoustic absorbing metamaterials [41,42]. The convolutional neural network (CNN) is a deep-learning model that efficiently extracts spatial features through the mechanisms of local receptive fields and weight sharing. We use a CNN to process the dataset generated via the finite-element method to correlate acoustic absorption spectra with structural configurations, allowing reverse engineering from the target absorption spectrum. Experimental results confirm the efficacy of this method, achieving broadband absorption at the target spectrum, with a material thickness around 1/13th of the wavelength at the lowest target frequency. This innovative integration marks a significant advancement in low-frequency-noise control strategies.

II. THEORETICAL MODEL AND NUMERICAL SIMULATION

To contextualize the practical applications delineated above within fundamental acoustical theory, a discussion of the interaction between acoustic waves and a material, quantified by acoustic impedance, is pertinent. Typically, acoustic impedance describes how the material reacts to external acoustic excitation. The absorption coefficient, α, of an acoustic metamaterial under normal incidence is calculated as follows:

$$\alpha = 1 - |R|^2 = 1 - \left|\frac{Z_H - Z_0}{Z_H + Z_0}\right|^2, \tag{1}$$

where $R = (Z_H - Z_0)/(Z_H + Z_0)$ is the reflection coefficient, Z_H is the acoustic impedance of the metamaterial, and $Z_0 = \rho_0 c_0$ is the characteristic impedance of the air. The density of air, ρ_0, is 1.21 kg/m^3, and the speed of sound in air, c_0, is 343 m/s. Equation (1) reveals that perfect absorption can be achieved when matched by the impedance of the metamaterial and air. This principle underpins the engineering of acoustic materials, where precise control of impedance is crucial for optimizing absorption performance.

Figure 1(a) depicts the proposed HPHR integrating sponges and a Helmholtz resonator, where the neck of the resonator is embedded. In the case of the HPHR described, the integration of sponges within the resonator is a strategic modification aimed at enhancing impedance matching, and thus, acoustic absorption. The dimensions are detailed in Fig. 1(b). It illustrates the unit as a cuboid with width W, depth D, height H, and total volume of the unit of $V_u = W \times D \times H$. The width of the neck is w, and its length is L. The wall thickness is represented by t, and d is the width of the air slit between the sponges. $\varphi_s = d/w$ is the porosity of the air slit. To analyze the behavior of acoustic waves within the neck, the bulk modulus, K_p, and density, ρ_p, of the porous materials are evaluated using the Johnson-Champoux-Allard (JCA) model of five parameters. The JCA model employs homogeneous material parameters to effectively characterize the behavior of sound-wave propagation within the porous medium [43]. The parameters of the porous material are shown in Table I. Employing effective-medium theory, we derive the effective parameters for the neck [44] schematically in Fig. 1(c), providing a comprehensive depiction of how the neck's material composition influences the overall acoustic characteristics of the HPHR. This theoretical approach allows us to model the acoustic impedance of the porous neck by treating it as a homogeneous medium with effective properties.

The acoustic impedance of the neck can be calculated similarly to that of microperforated panels [44]. Considering the terminal effects of the porous neck, the modified formula for calculating the acoustic impedance of HPHR is as follows [45]:

$$Z_H = \zeta \left[\frac{1}{\delta_N}\left(\frac{12\eta L}{w^2}k'_r + j\omega\rho_e L + \frac{1}{2}jF\omega\rho_e d\right) - j\,\frac{S\rho_0 c_0^2}{\omega V}\right], \tag{2}$$

where $\zeta = DW/(D-2t)(W-2t)$ is the acoustic impedance correction factor, considering the thickness of the unit wall; $\delta_N = w/(W-2t)$ is the perforation ratio of the face sheet. $\eta = 1.983 \times 10^{-5}$ Pa s is the dynamic viscosity of air, $k'_r = k_r + \frac{\sqrt{2}\beta w}{12l}$, and $\beta = \frac{w}{2}\sqrt{\omega\rho_e/\eta}$. $\sqrt{2}\beta w/12l$ and $(1/2)jF\omega\rho_e d$ are the correction terms caused by the end-sound radiation. The last term in square brackets is the impedance of the cavity. $\omega = 2\pi f$ is the angular frequency. ρ_e is the effective parameter of the neck elaborated in the Supplemental Material [44]. $j = \sqrt{-1}$ is the imaginary unit. F is the full elliptic integral of the first kind, which is relative to the ratio of w and $(D-2t)$. $S = (D-2t)(W-2t)$ is the area of the face sheet; $V = (D-2t)[(W-2t)(H-2t) - (w+2t)(L-t)]$ is the cavity volume after subtracting the neck volume from the unit volume.

To validate the above theoretical model, we employ the finite-element method using COMSOL Multiphysics. Since the thermoviscous losses occur in the porous materials [44], the "pressure acoustics, frequency domain" module is applied to the entire unit. The porous materials are characterized in the "poroacoustics domain" by the JCA model. The unit's dimensions are 50 mm for both width W and depth D, with a height (H) of 52 mm, and a wall thickness (t) of 1 mm. For the neck, the length of the neck is $L = 30$ mm, and $w = 4$ mm. φ_s takes values of 0.5, 0.625, 0.75, and 1. Figure 1(d) illustrates the absorption coefficient of the HPHR. The absorption coefficient declines gradually with an increase of φ_s, which is due to the decrease of thermal viscosity loss in the neck after the thickness of the sponge decreases. When $\varphi_s = 1$, the HPHR changes to a normal

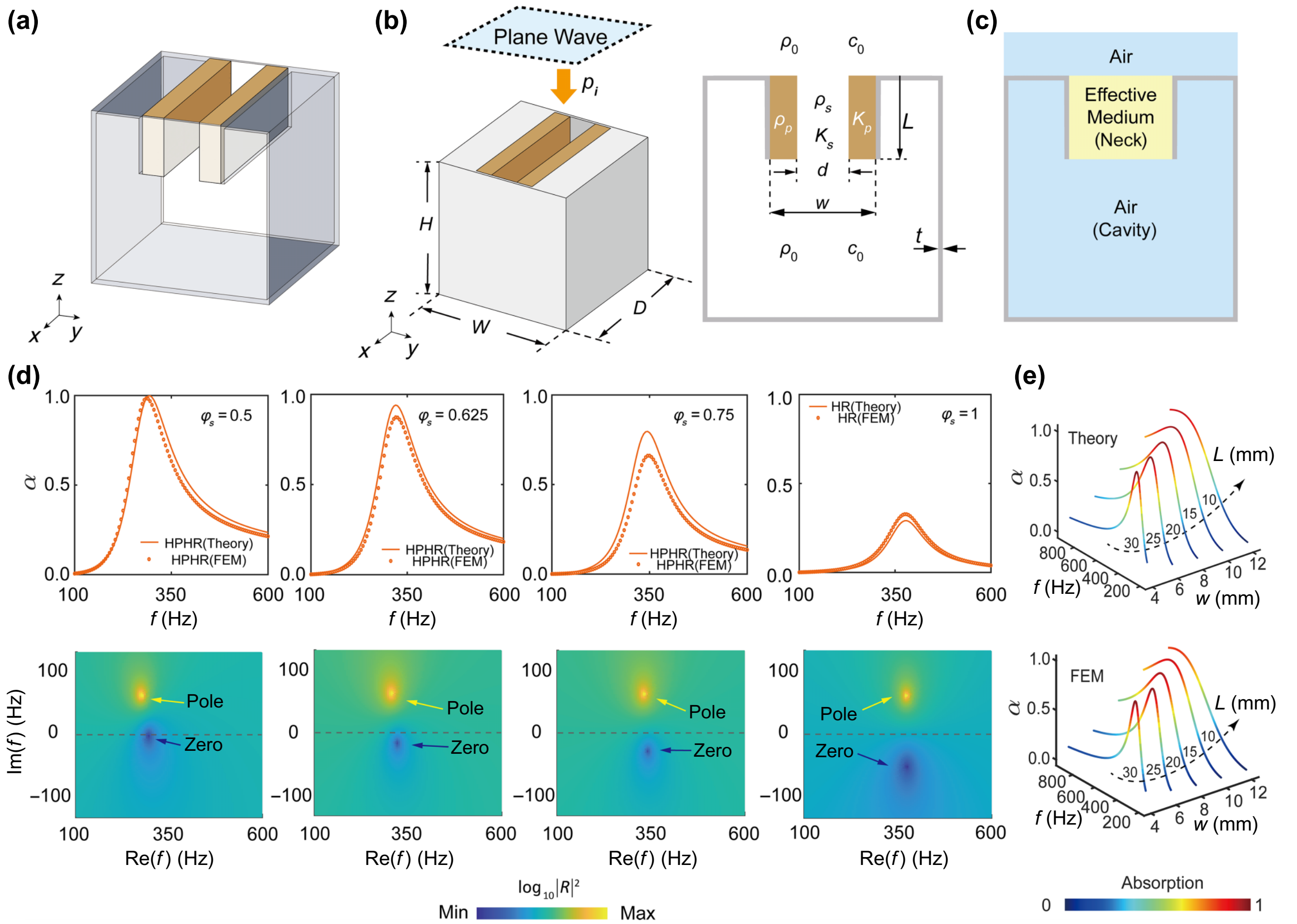

FIG. 1. (a) Schematic diagram of a hybrid porous Helmholtz resonator. (b) Dimensions and cross section in the x-axis direction of the HPHR. Sound wave is incident vertically on the face sheet. Material properties are labeled in the figure. (c) Effective-medium distribution in the HPHR. (d) Acoustic absorption coefficient and complex frequency-plane analysis for the HPHR under different φ_s. (e) Low-frequency absorption coefficients of the HPHR with various neck dimensions.

Helmholtz resonator. To simulate the absorption coefficient of Helmholtz resonators, the "acoustic-thermovisous acoustic interaction, frequency domain" module is utilized. Then, we adopt complex frequency-plane analysis to reveal the damping state of the HPHR intuitively [33]. For $\varphi_s = 0.5$, the zero point is located at the real axis [Im(f) is 0], which means that energy leakage of the system is balanced by the losses, consistent with the quasiperfect absorption. As the damping of the neck drops, the zero point and pole point shift down together. When the medium in the neck is just air ($\varphi_s = 1$), the Helmholtz resonator displays poor absorption due to insufficient energy dissipation. The results demonstrate the contribution of the porous structure on quasiperfect absorption, associated with acoustic impedance matching through modifying the damping state of the system [44].

TABLE I. Acoustic parameters of the porous material (melamine foam).

α_∞	ϕ	σ (N s/m^4)	Λ (µm)	Λ' (µm)
1.0059	0.995	10 500	240	470

The above results demonstrate that a porous neck is promising to reduce the resonant frequency while enhancing the system's energy loss to get a higher absorption coefficient. This adjustment implies that the HPHR has a better acoustic performance at lower frequencies compared to traditional Helmholtz resonators with the same thickness. To achieve efficient sound absorption across the low-frequency spectrum, we investigate HPHRs with varying neck dimensions (w varies from 4 to 12 mm in 2 mm increments, and L is adjusted from 30 to 10 mm in steps of -5 mm) with fixed $\varphi_s = 0.5$. The theoretical and simulation results, as illustrated in Fig. 1(e), demonstrate the HPHR's effective absorption in the low-frequency range, highlighting the critical role of the design parameters in achieving desired acoustic outcomes.

III. BROADBAND DESIGN AND EXPERIMENTAL DEMONSTRATION

To achieve broadband acoustic absorption, we develop a composite absorption structure comprising four parallel HPHRs, as illustrated in Fig. 2(a). Considering the design feasibility, each HPHR maintains an identical volume (V_u) and φ_s but varied w and L of the necks. The acoustic-electric analogy clarifies the role of each component in the HPHR for incident acoustic waves. It realizes nonlocal-resonance sound absorption by the coupling effect between adjacent unit cells. Determining the optimal combination of parameters across the four HPHRs increases the computational complexity. A more sophisticated method is required to efficiently navigate the vast parameter space and ensure that the final design achieves the desired acoustic performance. The application of advanced computational tools, like deep learning, is indispensable for finding the most suitable parameter set in low-frequency broadband absorption [46]. Among various deep-learning architectures, such as the CNN, the recurrent neural network (RNN), and transformers [47–49], the CNN is particularly effective due to its ability to extract features from complex datasets at a lower computational cost and faster speed [42,50,51]. In this context, we propose to employ a one-dimensional (1D) CNN to design the absorbing structures inversely from the target acoustic absorption curve. The model is depicted in Fig. 2(b). It aims to establish the mapping between geometric parameters L_n and the features of the sound-absorption spectrum. This approach will allow for direct mapping from the desired acoustic performance to the optimal parameter set, bypassing the limitations posed by traditional theoretical and numerical methods [41]. The model incorporates a

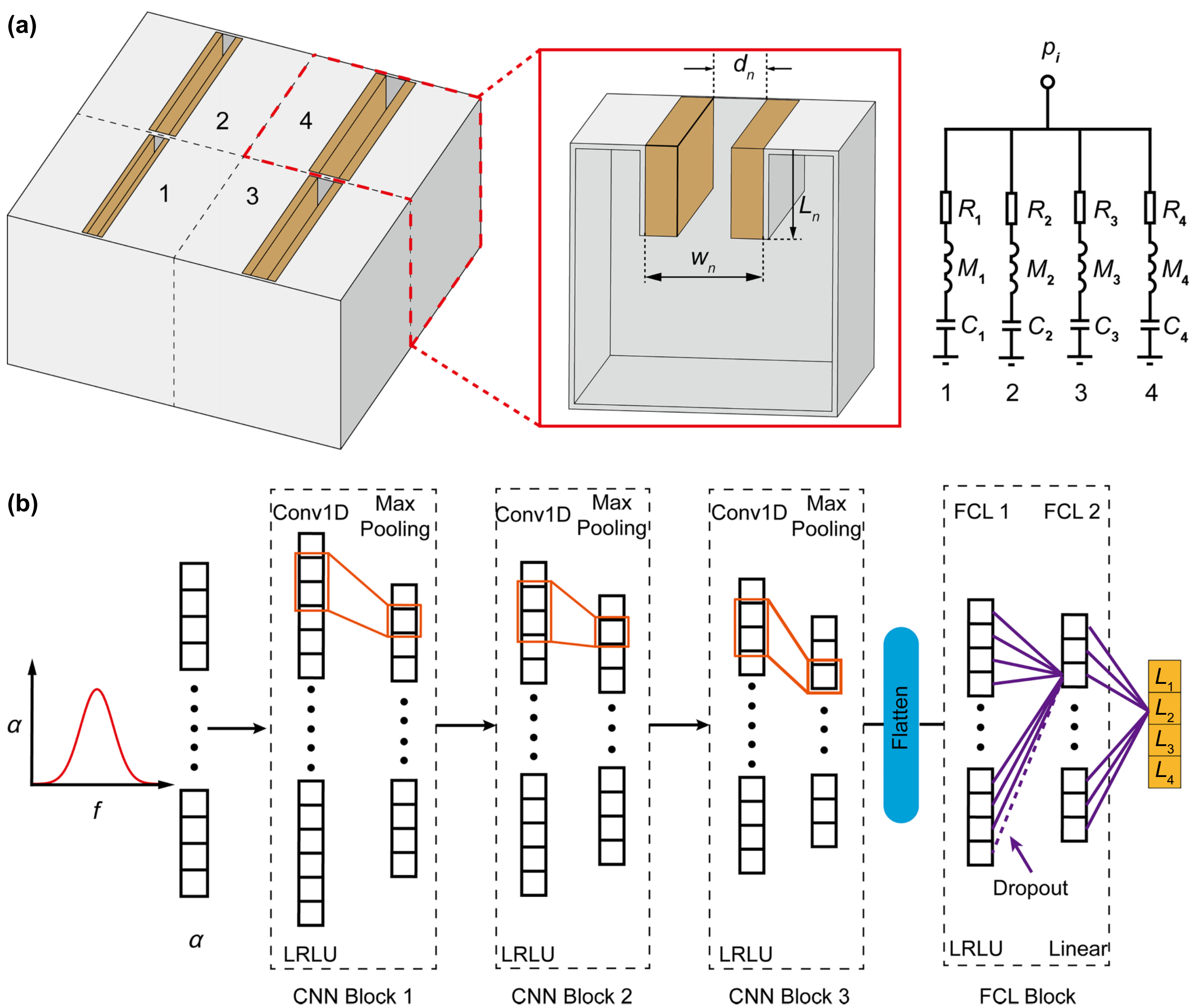

FIG. 2. (a) Schematic diagram of the composite absorption structure consisting of HPHRs (left) and equivalent circuit models (right). (b) 1D-CNN model for inverse design of the acoustic metamaterial.

maximum pooling layer following each 1D-CNN layer to reduce computational load and improve model generalization. The maximum pooling layer slides over the input data, selecting the maximum value within each window for output. The activation function is a leaky rectified linear unit (LRLU) in the CNN architectures. After feature extraction in CNN blocks, the fully connected layer (FCL) identifies features after the flatten operation. It obtains the associations between features and finally maps them onto the output space. To mitigate overfitting, a dropout operation is introduced within the FCLs. It reduces the interactions between features, thereby minimizing local feature dependency and enhancing the model's generalizability.

To ensure the quality of the dataset and prevent redundancy, the neck widths w_1–w_4 are fixed to 6, 8, 10, and 12 mm. The neck lengths L_1–L_4 are treated as labels and represented as structural vectors $L = (L_1, L_2, L_3, L_4)$. The acoustic absorption spectrum is encoded as $A = (\alpha_1, \alpha_2, \ldots, \alpha_{71})$, covering frequencies from 200 to 900 Hz in steps of 10 Hz. A total of 10 000 pairs of absorption spectra and structural vectors constitute the dataset. We allocate 70% of the dataset for training and 30% for testing. The model

TABLE II. Part predictions of structures based on CNN.

	L_1 (mm)	L_2 (mm)	L_3 (mm)	L_4 (mm)
Prediction1(Pre1)	4.92	12.53	30.31	8.28
Prediction2(Pre2)	2.72	11.51	26.95	8.71
Prediction3(Pre3)	4.43	11.2	25.97	13.35

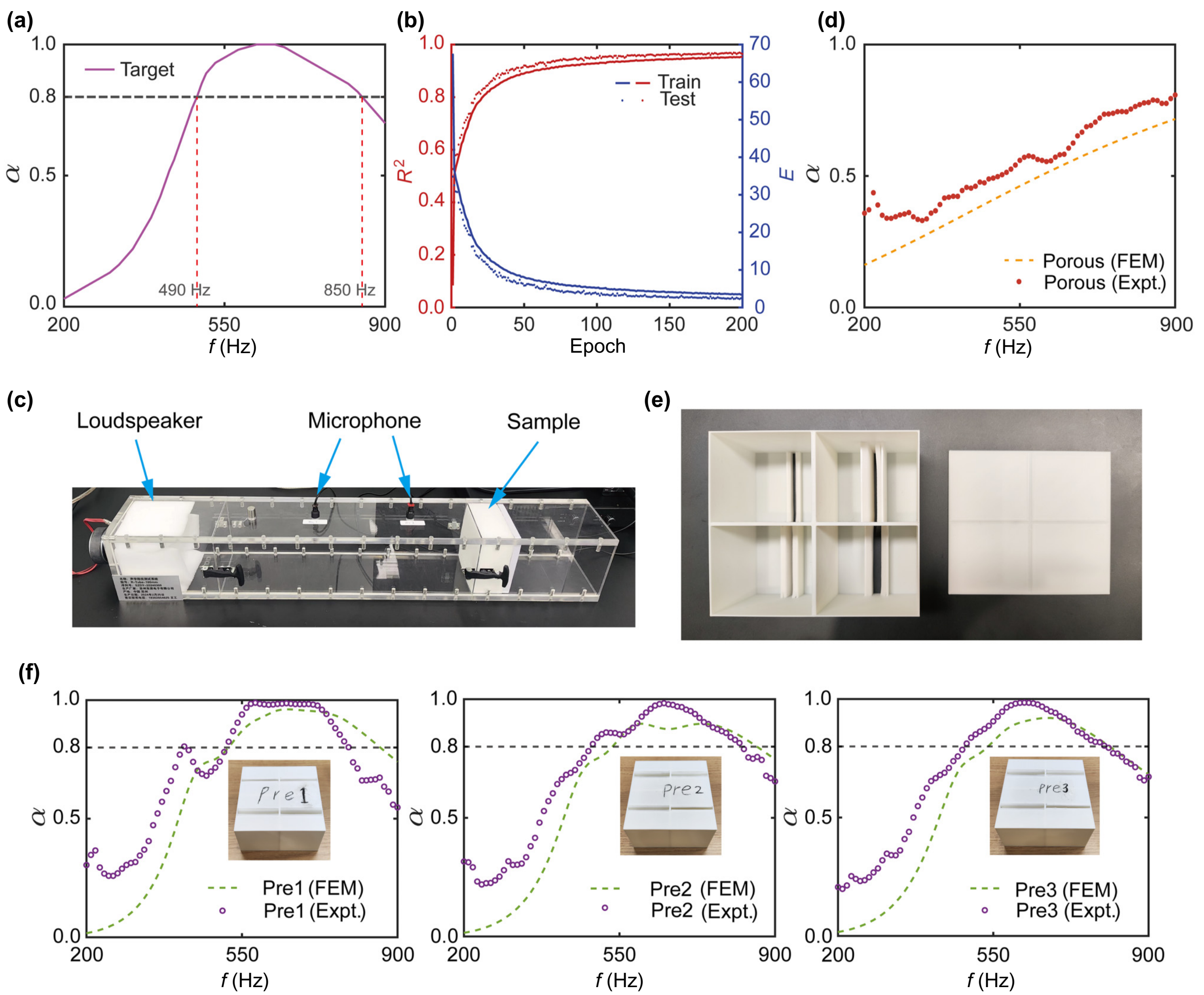

FIG. 3. (a) Target acoustic absorption spectrum. (b) Loss curves (E) and R^2 coefficients of train and test sets. (c) Experimental setup of the SZDY R-Tube 100-mm impedance tube testing system. (d) Sound-absorption coefficient of porous materials. (e) Photograph of the 3D-printed specimen and its inner structure. (f) Simulated (green dotted lines) and measured (purple circles) acoustic absorption coefficients of the optimized composite absorption structure. Inset shows a top view of a 3D-printed specimen.

is implemented on the Anaconda3 platform using PYTHON version 3.7 and it employs the Keras framework with the TensorFlow backend. The target absorption spectrum, as shown in Fig. 3(a), is inputted into the model to assess the CNN model's performance, aiming for an absorption coefficient above 0.8 between 490 and 850 Hz (about 0.8 octave). Figure 3(b) presents R^2 coefficients and the loss function mean squared error (MSE) curves. The coefficient of determination, R^2, is used to evaluate the performance of our model:

$$R^2 = 1 - \frac{\sum_i (Y_i - \hat{Y}_i)^2}{\sum_i (Y_i - \bar{Y}_i)^2}, \tag{3}$$

where Y_i denotes the network output, $\hat{Y}_i$ denotes the corresponding label, and $\bar{Y}_i$ denotes the average value of the corresponding label. R^2 is a number between 0 and 1 that measures how well a statistical model predicts an outcome. The better a model is at making predictions, the closer its R^2 will be to 1. The loss-function E is used as an objective function to minimize the difference between the output and the set of labels:

$$E = \frac{1}{m}\sum_{i=1}^{m} (Y_i - \hat{Y}_i)^2, \tag{4}$$

where m denotes the number of samples. As the E decreases, the absorption spectrum of the optimized structure increasingly aligns with the target value, indicating improved predictive performance of the model. After 200 epochs, R^2 coefficients for training and testing are finally stabilized above 0.95 with the significant decay of E, demonstrating satisfactory performance and high accuracy of the model. Parts from the predictions are displayed in Table II.

Based on predictions, we perform an experimental validation and compare it with the finite-element results. As a comparative validation, we first measured the melamine foam to demonstrate the superiority of the structure in low-frequency acoustic performance. The thickness of the foam is 52 mm, and the cross section is 100×100 mm^2. The experimental tests are conducted using the SZDY R-Tube 100-mm impedance tube testing system, as shown in Fig. 3(c). The tests cover a frequency range from 200 to 900 Hz. The absorption coefficient of melamine foam is shown in Fig. 3(d). Compared with the finite-element method (FEM) result, the measurement shows a slight deviation. This may be due to the inhomogeneity of the melamine foam parameters induced by machining error. In addition, the force applied to the sample during the test can also change the parameters of the melamine foam, affecting the sound-absorption measurements.

Three optimized composite absorption structures are fabricated via three-dimensional (3D) printing for experimental validation. The size of the sample is $100 \times 100 \times 52$ mm^3. The schematic of the internal structure is depicted in Fig. 3(e). Melamine foam is glued to the neck of HPHRs. The results, presented in Fig. 3(f), display minimal deviation between experimental and FEM ones. Experimental measurements validate our design approach to a large extent. Three samples achieve broadband absorption exceeding 0.8 near the target spectrum, confirming the design's effectiveness and its robust low-frequency broadband absorption capability. The thickness of the samples is approximately 1/13th of the wavelength at the lowest target frequency. We further investigated the oblique incidence at angles less than 40° [44], and the absorption performance remained robust. Furthermore, we conducted a simulation study on the sound-absorption characteristics of the optimized structure in a lower-frequency range (350–510 Hz), and the results also validated the effectiveness of our HPHR model [44].

IV. CONCLUSIONS

We propose a HPHR that integrates porous materials into the neck, thereby modifying and tuning the effective acoustic parameters of the resonator. The sound absorption performance of the HPHR is investigated through theoretical analysis and FEM simulations. By adjusting the proportion of porous material in the neck, efficient low-frequency acoustic absorption can be achieved without altering the physical dimensions of the metamaterial. This approach significantly enhances the acoustic absorption capabilities of the system. Additionally, we designed a composite absorption structure based on parallel HPHRs, which was optimized using a 1D CNN. This design yields robust and efficient sound absorption across the target broadband spectrum, achieving absorption efficiencies exceeding 0.8 within the desired bandwidth. The thickness of this composite structure is approximately 1/13th of the wavelength at the lowest target frequency. This work highlights the potential of the HPHR to advance broadband structural design at subwavelength scales with improved low-frequency noise control.

Data that support the findings of this study are available from the corresponding author upon reasonable request.

ACKNOWLEDGMENTS

The authors thank Professor Yong Li for his valuable discussions. This work is supported by the National Key Research and Development Program of China (Grant No. 2023YFA1406900).

The authors declare no conflict of interest.

[1] Y. Champoux and J.-F. Allard, Dynamic tortuosity and bulk modulus in air-saturated porous media, J. Appl. Phys. **70**, 1975 (1991).

[2] M. R. Stinson and Y. Champoux, Propagation of sound and the assignment of shape factors in model porous materials having simple pore geometries, J. Acoust. Soc. Am. **91**, 685 (1992).

[3] S. R. Pride, F. D. Morgan, and A. F. Gangi, Drag forces of porous-medium acoustics, Phys. Rev. B **47**, 4964 (1993).

[4] C. Gaulon, J. Pierre, C. Derec, L. Jaouen, F.-X. Bécot, F. Chevillotte, F. Elias, W. Drenckhan, and V. Leroy, Acoustic absorption of solid foams with thin membranes, Appl. Phys. Lett. **112**, 261904 (2018).

[5] D. L. Johnson, J. Koplik, and R. Dashen, Theory of dynamic permeability and tortuosity in fluid-saturated porous media, J. Fluid Mech. **176**, 379 (1987).

[6] X. Olny and C. Boutin, Acoustic wave propagation in double porosity media, J. Acoust. Soc. Am. **114**, 73 (2003).

[7] Z. Liu, X. Zhang, Y. Mao, Y. Y. Zhu, Z. Yang, C. T. Chan, and P. Sheng, Locally Resonant Sonic Materials, Science **289**, 1734 (2000).

[8] Y. Zhu, F. Fei, S. Fan, L. Cao, K. Donda, and B. Assouar, Reconfigurable origami-inspired metamaterials for controllable sound manipulation, Phys. Rev. Appl. **12**, 034029 (2019).

[9] Y. Zhu, S.-W. Fan, L. Cao, K. Donda, and B. Assouar, Acoustic meta-equalizer, Phys. Rev. Appl. **14**, 014038 (2020).

[10] Xudong Fan, Yifan Zhu, Zihao Su, Ning Li, Xiaolong Huang, Yang Kang, Can Li, Chunsheng Weng, Hui Zhang, Weiwei Kan, and Badreddine Assouar, Transverse particle trapping using finite Bessel beams based on acoustic metamaterials, Phys. Rev. Appl. **19**, 034032 (2023).

[11] M. Yang, G. Ma, Z. Yang, and P. Sheng, Subwavelength perfect acoustic absorption in membrane-type metamaterials: a geometric perspective, EPJ Appl. Metamater. **2**, 10 (2015).

[12] F. Ma, C. Wang, Y. Du, Z. Zhu, and J. H. Wu, Enhancing of broadband sound absorption through soft matter, Mater. Horiz. **9**, 653 (2022).

[13] Z. Xiao, P. Gao, X. He, Y. Qu, and L. Wu, Lightweight cellular multifunctional metamaterials with superior low-frequency sound absorption, broadband energy harvesting and high load-bearing capacity, Mater. Des. **241**, 112912 (2024).

[14] D.-Y. Maa, Potential of microperforated panel absorber, J. Acoust. Soc. Am. **104**, 2861 (1998).

[15] V. Romero-García, G. Theocharis, O. Richoux, A. Merkel, V. Tournat, and V. Pagneux, Perfect and broadband acoustic absorption by critically coupled sub-wavelength resonators, Sci. Rep. **6**, 19519 (2016).

[16] S. Huang, X. Fang, X. Wang, B. Assouar, Q. Cheng, and Y. Li, Acoustic perfect absorbers via Helmholtz resonators with embedded apertures, J. Acoust. Soc. Am. **145**, 254 (2019).

[17] Z. Su, H. Luo, S. Gao, Z. Luo, Y. Zhu, and H. Zhang, Customizable acoustic metamaterial barrier with intelligent sound insulation, Phys. Rev. Appl. **18**, 064029 (2022).

[18] Y. Guan, Y. Ge, C. Wu, Q. Si, Y. Lai, S. Yuan, and H. Sun, An ultra-low-frequency sound absorber and its application in noise reduction in ducts, APL Mater. **12**, 011127 (2024).

[19] C. Chen, Z. Du, G. Hu, and J. Yang, A low-frequency sound absorbing material with subwavelength thickness, Appl. Phys. Lett. **110**, 221903 (2017).

[20] S. Qu, N. Gao, A. Tinel, B. Morvan, V. Romero-García, J.-P. Groby, and P. Sheng, Underwater metamaterial absorber with impedance-matched composite, Sci. Adv. **8**, eabm4206 (2022).

[21] X. Zhang, Y. Ye, Y. Lu, and X. Wang, A design method for accurate acoustic impedance matching under coherent coupling of sound-absorbing subunits, J. Appl. Phys. **133**, 204903 (2023).

[22] S. Y. Song, X. H. Yang, F. X. Xin, S. W. Ren, and T. J. Lu, Modeling of roughness effects on acoustic properties of micro-slits, J. Phys. D: Appl. Phys. **50**, 235303 (2017).

[23] M. Duan, C. Yu, Z. Xu, F. Xin, and T. J. Lu, Acoustic impedance regulation of Helmholtz resonators for perfect sound absorption via roughened embedded necks, Appl. Phys. Lett. **117**, 151904 (2020).

[24] L. Zhang, W. Zhang, and F. Xin, Sound absorption of two-dimensional rough tube porous materials, Phys. Fluids **34**, 083612 (2022).

[25] J. Yang, J. S. Lee, and Y. Y. Kim, Metaporous layer to overcome the thickness constraint for broadband sound absorption, J. Appl. Phys. **117**, 174903 (2015).

[26] Y. Zhou, D. Li, Y. Li, and T. Hao, Perfect acoustic absorption by subwavelength metaporous composite, Appl. Phys. Lett. **115**, 093503 (2019).

[27] H. Zhao, Y. Wang, D. Yu, H. Yang, J. Zhong, F. Wu, and J. Wen, A double porosity material for low frequency sound absorption, Compos. Struct. **239**, 111978 (2020).

[28] F. An, P. Zhao, X. Li, Q. Wu, and B. Liu, Active impedance control of a loudspeaker and its parallel combination with porous materials for broadband sound absorption, Mech. Syst. Signal Process. **206**, 110909 (2024).

[29] X. Liu, X. Ma, C. Yu, and F. Xin, Sound absorption of porous materials perforated with holes having gradually varying radii, Aerosp. Sci. Technol. **120**, 107229 (2022).

[30] W. Zhang, X. Liu, and F. Xin, Sound absorption performance of helically perforated porous metamaterials at high temperature, Mater. Des. **225**, 111437 (2023).

[31] X. Liu, M. Liu, and F. Xin, Sound absorption of a perforated panel backed with perforated porous material: Energy dissipation of Helmholtz resonator cavity, Mech. Syst. Signal Process. **185**, 109762 (2023).

[32] W. Zhang and F. Xin, Broadband low-frequency sound absorption via Helmholtz resonators with porous material lining, J. Sound Vib. **578**, 118330 (2024).

[33] V. Romero-García, G. Theocharis, O. Richoux, and V. Pagneux, Use of complex frequency plane to design broadband and sub-wavelength absorbers, J. Acoust. Soc. Am. **139**, 3395 (2016).

[34] M. Yang, S. Chen, C. Fu, and P. Sheng, Optimal sound-absorbing structures, Mater. Horiz. **4**, 673 (2017).

[35] H. Ding, X. Fang, B. Jia, N. Wang, Q. Cheng, and Y. Li, Deep learning enables accurate sound redistribution via nonlocal metasurfaces, Phys. Rev. Appl. **16**, 064035 (2021).

[36] Y. Zhu, A. Merkel, K. Donda, S. Fan, L. Cao, and B. Assouar, Nonlocal acoustic metasurface for ultrabroadband sound absorption, Phys. Rev. B **103**, 064102 (2021).

[37] B. Lusch, J. N. Kutz, and S. L. Brunton, Deep learning for universal linear embeddings of nonlinear dynamics, Nat. Commun. **9**, 4950 (2018).

[38] A. D. Tranter, H. J. Slatyer, M. R. Hush, A. C. Leung, J. L. Everett, K. V. Paul, P. Vernaz-Gris, P. K. Lam, B. C. Buchler, and G. T. Campbell, Multiparameter optimisation of a magneto-optical trap using deep learning, Nat. Commun. **9**, 4360 (2018).

[39] X. Lin, Y. Rivenson, N. T. Yardimci, M. Veli, Y. Luo, M. Jarrahi, and A. Ozcan, All-optical machine learning using diffractive deep neural networks, Science **361**, 1004 (2018).

[40] J. Weng, Y. Ding, C. Hu, X.-F. Zhu, B. Liang, J. Yang, and J. Cheng, Meta-neural-network for real-time and passive deep-learning-based object recognition, Nat. Commun. **11**, 6309 (2020).

[41] K. Donda, Y. Zhu, A. Merkel, S.-W. Fan, L. Cao, S. Wan, and B. Assouar, Ultrathin acoustic absorbing metasurface based on deep learning approach, Smart Mater. Struct. **30**, 085003 (2021).

[42] L. Liu, L.-X. Xie, W. Huang, X. J. Zhang, M.-H. Lu, and Y.-F. Chen, Broadband acoustic absorbing metamaterial via deep learning approach, Appl. Phys. Lett. **120**, 251701 (2022).

[43] M. Yang and P. Sheng, Sound absorption structures: From porous media to acoustic metamaterials, Annu. Rev. Mater. Res. **47**, 83 (2017).

[44] See the Supplemental Material at http://link.aps.org/supplemental/10.1103/PhysRevApplied.22.044032, which includes Refs. [1,2,5,6], for the effective parameters and acoustic impedance of the HPHR, the effect of thermoviscous losses, the parameter configuration of the 1D CNN, and the performance verification under oblique incidence and frequencies below 500 Hz.

[45] D.-Y. Maa, *Fundamentals of Modern Acoustic Theory* (Science Press, Beijing, 2004).

[46] K. Donda, Y. Zhu, A. Merkel, S. Wan, and B. Assouar, Deep learning approach for designing acoustic absorbing metasurfaces with high degrees of freedom, Extreme Mech. Lett. **56**, 101879 (2022).

[47] Y. LeCun, B. Boser, J. S. Denker, D. Henderson, R. E. Howard, W. Hubbard, and L. D. Jackel, Backpropagation applied to handwritten zip code recognition, Neural Comput. **1**, 541 (1989).

[48] A. Vaswani, N. Shazeer, N. Parmar, J. Uszkoreit, L. Jones, A. N. Gomez, L. Kaiser, and I. Polosukhin, Attention is all you need, arXiv:1706.03762.

[49] E. Zea, E. Brandão, M. Nolan, J. Cuenca, J. Andén, and U. P. Svensson, Sound absorption estimation of finite porous samples with deep residual learning, J. Acoust. Soc. Am. **154**, 2321 (2023).

[50] O. Abdeljaber, O. Avci, S. Kiranyaz, M. Gabbouj, and D. J. Inman, Real-time vibration-based structural damage detection using one-dimensional convolutional neural networks, J. Sound Vib. **388**, 154 (2017).

[51] M. Rautela, S. Gopalakrishnan, K. Gopalakrishnan, and Y. Deng, in 2020 IEEE International Conference on Prognostics and Health Management (ICPHM) (IEEE, Detroit, MI, USA, 2020), pp. 1–7.